Int. J. Electrochem. Sci., 13 **(2018)** 8030 – 8041, doi: 10.20964/2018.08.62

International Journal of
ELECTROCHEMICAL
SCIENCE
www.electrochemsci.org

Preparation of Cr-Ni Alloy by Electrochemical Codeposition in a NaCl-KCl-NaF-Cr_2O_3-NiO Molten Salt

Shixian Zhang[1,2], *Yungang Li*[1,*], *Kai Hu*[3], *Xiaoping Zhao*[2], *Hui Li*[1], *Jinglong Liang*[1]

[1] Key Laboratory of Ministry of Education for Modern Metallurgy Technology, College of Metallurgy and Energy, North China University of Science and Technology, 21# Bohai Road, Caofeidian Xincheng, Tangshan 063210, China
[2] Hebei College of Industry and Technology, 626# Hongqi Street, Shijiazhuang 050091, China
[3] School of Materials Science and Engineering, Chongqing University, 174# Shazhengjie, Shapingba, Chongqing 400044, China
[*]E-mail: liyungang59322@163.com

Received: 22 April 2018 / *Accepted:* 2 June 2018 / *Published:* 5 July 2018

The feasibility of electrochemical reduction in a NaCl-KCl-NaF-Cr_2O_3-NiO molten salt is analysed by thermodynamic calculation. The electrochemical reaction mechanism and the electrocrystallization process of chromium and nickel in the same molten salt are investigated at 1073 K by electrochemical workstation. Cyclic voltammetry, chronopotentiometry and chronoamperometry have been used. The results show that it is thermodynamically feasible to reduce NiO and Cr_2O_3 to pure metal by electrochemical reduction and indicate that the electrochemical reduction from Cr(III) to Cr takes two steps: $Cr^{3+} + e \rightarrow Cr^{2+}$ and $Cr^{2+} + 2e \rightarrow Cr$. Meanwhile, the electrochemical reduction from Ni(II) to Ni takes only one step: $Ni^{2+} + 2e \rightarrow Ni$. All the electrochemical processes of Cr(III), Cr(II) and Ni(II) are reversible reactions, and the electrocrystallization processes of Cr and Ni are an instantaneous hemispheroid three-dimensional nucleation process. The atomic growth process, composition and morphology of the coating are investigated by SEM and EDS, and close and uniform alloy particles are deposited on the substrate. The polarization curves are determined by the potentiodynamic scanning method, and the results show that the corrosion reaction of the alloy coating is higher, and the corrosion rate is lower. It is also found that the corrosion resistance of the Cr-Ni alloy coating is stronger than that of low carbon steel.

Keywords: Cr-Ni alloy, coating, electrochemical codeposition, molten salt, characterization

1. INTRODUCTION

Because of the excellent corrosion, abrasion, oxidation resistance and high thermal strength properties, chromium-nickel alloy is widely used in nuclear, aviation, chemical industries, etc.[1,2]. Almost all these types of alloys are smelted in high-temperature furnaces by using high-purity raw

materials. Both Cr and Ni are precious and expensive metals. Therefore, an economical manufacturing process is of great concern. Electrodeposition technology is one of the important techniques with low cost, small technical obstacles and flexible process. Many researchers have prepared chromium-nickel alloys by using the electrodeposition technology[3,4] or metallurgy[5-8]. When the chromium content reaches a certain value in the nickel-chromium alloy, a non-crystalline nickel-chromium structure will form with high corrosion resistance and is even better than stainless steel with the same chromium content on the surface. In addition, the chromium-nickel alloy plating metal material will form a chromium passivation film. When the chromium content in the passivation film is greater than 20%, the corrosion resistance of the base material will be improved. It will reduce the consumption of stainless steel and can save nickel and chromium resources. Due to the high melting point and high price of chromium and nickel and the toxicity of hexavalent chromium, the application of chromium-nickel alloys is limited. The molten salt electrochemical method is applied in the reduction process of oxide powder, and the most representative one is the FFC Cambridge technology. Electrode oxidation of solid metal oxides in molten salts is a relatively new and versatile reduction method, not only for the extraction of active metals but also for the synthesis of many functional alloys and inorganic materials. There are many research fields in the preparation of various metals and alloys, such as chromium[9] and Fe-Ni[10]. However, less research has been conducted on the preparation of chromium-nickel alloys using molten salt electrodeposition.

A Cr-Ni alloy coating prepared by the electrodeposition method in a NaCl-KCl-NaF-Cr_2O_3-NiO molten salt is proposed. The electrochemical reduction and the nucleation mechanism of Cr(III) and Ni(II) in the molten salt were studied. Nickel-chromium alloy coating was prepared by the electrodeposition technology, and its electrochemical corrosion performance was studied.

2. EXPERIMENTS

2.1 Theoretical calculation

The thermodynamic data of molten salt electrochemical reduction were calculated using HSC7.0 software, which was designed by Outokumpu Research Oy in Finland.

2.2 Materials

All analytically pure reagents were weighed with a molar ratio of X_{NaCl}:X_{KCl}:X_{NaF}:X_{Cr2O3}:X_{NiO} = 0.64:0.64:0.32:0.01:0.01 and mixed. The mixed salt was ground with an agate mortar and heated at 473 K for 12 hours.

2.2 Electrocrystallization

The dried reagent was placed in a high-purity zirconia crucible and placed in a resistance furnace. The furnace temperature was controlled by an artificial intellective controller (Model: AI-808p) and measured by a thermocouple (Model: S) with an accuracy of ±1°C. The furnace was airtight

so that the experiment could be performed in an inert atmosphere of high-purity argon gas. The NaCl-KCl-NaF, NaCl-KCl-NaF-Cr_2O_3 and NaCl-KCl-NaF-Cr_2O_3-NiO molten salts were preserved isothermally for 7 hours at 1073 K.

Pre-electrolysis was performed for 2 hours at a constant voltage of 2 V to remove residual water, oxide anions, and other compounds. The experiment of molten salt electrochemistry was carried out by Zahner workstation (Model: IM6eX, Germany), using the traditional three-electrode cell configuration. The working electrode, reference electrode and counter electrode were all made of platinum wire with a diameter of 0.5 mm (99.99%). An alumina tube having an inner diameter of 0.6 mm was used as the sleeve. The three electrodes were soaked in concentrated hydrochloric acid for 1 minute and shaken with an ultrasonic cleaner containing deionized water and ethanol for 5 minutes. They were dried with a blower before each experiment. The CVs of NaCl-KCl-NaF, NaCl-KCl-NaF-Cr_2O_3 and NaCl-KCl-NaF-Cr_2O_3-NiO were measured using a scanning speed of 0.5 V/s at 1073 K. The CVs of NaCl-KCl-NaF-Cr_2O_3-NiO were measured between the scanning speed 0.3 V/s and 0.5 V/s (step of 0.05 V/s) at 1073 K. The chronopotentiograms of the NaCl-KCl-NaF-Cr_2O_3-NiO molten salt were measured with a constant current of 250 mA at 1073 K. The chronoamperometry curves of the NaCl-KCl-NaF-Cr_2O_3-NiO molten salt were measured in the potential range of -0.33 V to -0.98 V.

2.4 Coelectrodeposition

According to the results of the electrochemical experiments, a 20 mm×20 mm×1 mm platinum sheet was used as an electrode, and the electrodeposition experiment was performed in the molten salt. The platinum sheet electrodes were polished with silicon carbide sandpaper (320, 500, 1000, 1500, and 2000 mesh) and then degreased by immersing in 5% NaOH solution for 5 min. The pickling was soaked in 5% hydrochloric acid solution for 5 minutes, then rinsed in an ultrasonic cleaner for 5 minutes with ethanol, and blown dry with a blower for later use. Electrodeposition experiment was performed using the processed platinum sheet.

2.5 Analysis and detection

The surface morphology and chemical composition of the working electrode were observed by FEI, Quanta, 650 FEG field emission scanning electron microscopy (SEM) and its auxiliary energy dispersive X-ray spectroscopy (EDS). The corrosion resistance of the chromium-nickel alloy coating was determined by the anodic polarization curve measured by the dynamic scanning method with a scanning speed of 50 $mV \cdot min^{-1}$ at 25℃ in 3.5% NaCl solution.

3. RESULTS AND DISCUSSION

3.1 Thermodynamic analysis

The thermodynamics of the pure metals was calculated using the HSC thermodynamics software, and the theoretical decomposition voltage (E^{θ}) was calculated according to equation (1)[11].

$\Delta G^{\theta}=-nFE^{\theta}$ (1)

where $\triangle G^{\theta}$ is the standard Gibbs free energy change ($kJ\cdot mol^{-1}$), n is the electron transfer number and F is the Faraday's constant (96485 $C\cdot mol^{-1}$). As shown in Fig. 1, the theoretical decomposition voltages of NaCl, KCl and NaF are -3.23 V, -3.48 V and -4.81 V at 1073 K, respectively. In the reactions of (2)-(5), the theoretical decomposition voltage of NiO to Ni is the highest. Therefore, Ni is first reduced in the molten salt. Reactions (6)-(10) are likely to occur when Cr_2O_3 is reduced to metal Cr. It can be seen that Cr_2O_3 directly generating Cr or Cr_2O requires a large cell voltage, so these two reactions are difficult to occur. Therefore, reaction (10) does not occur as a follow-up reaction. Compared to the other reactions, the deposition potentials of reactions (7) and (8) are very low and are most likely to occur. According to the comparison of the thermodynamic equilibrium potentials, the electrochemical processes of NiO and Cr_2O_3 reduction to pure metal in NaCl-KCl-NaF-NiO-Cr_2O_3 molten salt are feasible.

Through thermodynamic software analysis, CrO is found to be metastable. Theoretically, Cr_2O_3 is first adsorbed on the surface of the electrode and then reduced to CrO, followed by CrO being rapidly reduced to Cr.

$2NaCl=2Na+Cl_2$ （2）

$2KCl=2K+Cl_2$ （3）

$2NaF=2Na+F_2$ （4）

$2NiO=2Ni+O_2$ （5）

$Cr_2O_3=2Cr+1.5O_2$ （6）

$Cr_2O_3=2CrO(g)+0.5O_2$ （7）

$2CrO(g)=2Cr+O_2$ （8）

$Cr_2O_3=Cr_2O(g)+O_2$ （9）

$2Cr_2O(g) = 4Cr + O_2(g)$ （10）

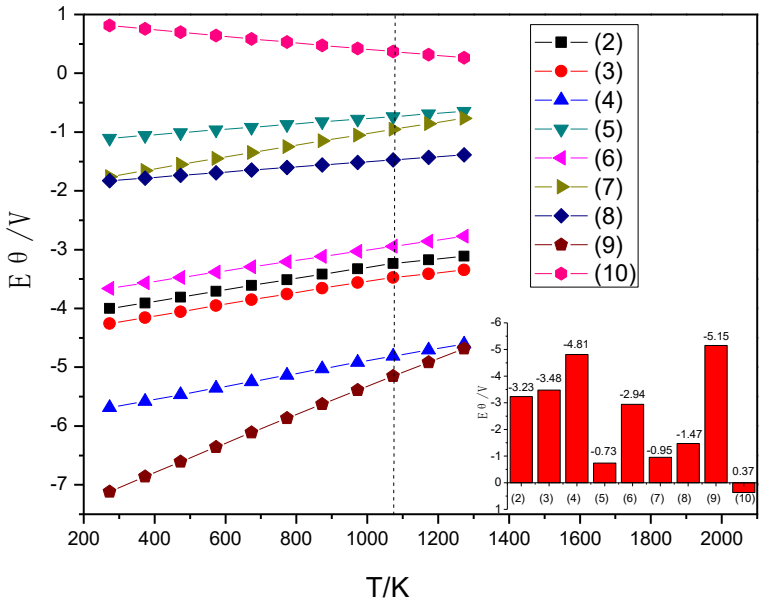

Figure 1. Theoretical decomposition voltages of all chemical reactions in NaCl-KCl-NaF-NiO-Cr_2O_3 molten salt (Insert: the theoretical decomposition voltages of all chemical reactions at 1073 K)

3.2 Cyclic voltammetry

Fig. 2 shows the typical CVs of NaCl-KCl-NaF, NaCl-KCl-NaF-Cr_2O_3 and NaCl-KCl-NaF-Cr_2O_3-NiO using a platinum electrode at 1073 K. The blue curve is a cyclic voltammogram of NaCl-KCl-NaF molten salt. This shows that there is no redox reaction between -1.2 V and 0.3 V because there is no cathode/anode reaction. The black curve is a cyclic voltammogram of NaCl-KCl-NaF-Cr_2O_3 molten salt. As seen in the curve, there are two pairs of cathode/anode (A/a and B/b) peaks corresponding to the deposited and dissolved Cr. The difference of the theoretical decomposition voltage agrees with that of the actual decomposition voltage. This shows that Cr(III) is reduced to metallic chromium by two-step electron transfer reactions. In the negative scan, peak b is the conversion process of Cr(III) to Cr(II), and peak a is the conversion process of Cr(II) to Cr. In the positive scan, peaks A and B are the transitions of Cr to Cr(II) and Cr(II) to Cr(III); this finding is consistent with the research of Giovanardi[12]. The red curve is a cyclic voltammogram of NaCl-KCl-NaF-Cr_2O_3-NiO molten salt. Another couple of cathodic/anodic (C'/c') signals occur except for the primary signals A'/a' and B'/b'. The reduction potential of Cr(III) to Cr(II) is -0.611 V, and the reduction potential of Cr(II) to Cr is -0.956 V. The result is close to the result of the cyclic voltammogram in NaCl-KCl-NaF-Cr_2O_3 molten salt. Moreover, the decomposition voltages between reactions (5) to (7) and (5) to (8) are generally consistent with the difference of the actual decomposition voltages. It is inferred that peak c' is the reduction of Ni.

At the same time, another signal (d') was detected in the black and red curves. Oxygen ingression during heating and incubation may cause Cr_2O_3 to be oxidized to some high-valence oxides. The ΔG of Cr_2O_3 to CrO_3 is the lowest in the reactions for forming high-valent oxides, so it is judged that this reaction is most likely to occur. Additionally, the difference between the decomposition voltage of d' to b' and d' to a' is consistent with that of the theoretical decomposition voltage. It can be concluded that peak d' is the reduction of CrO_3 to Cr_2O_3.

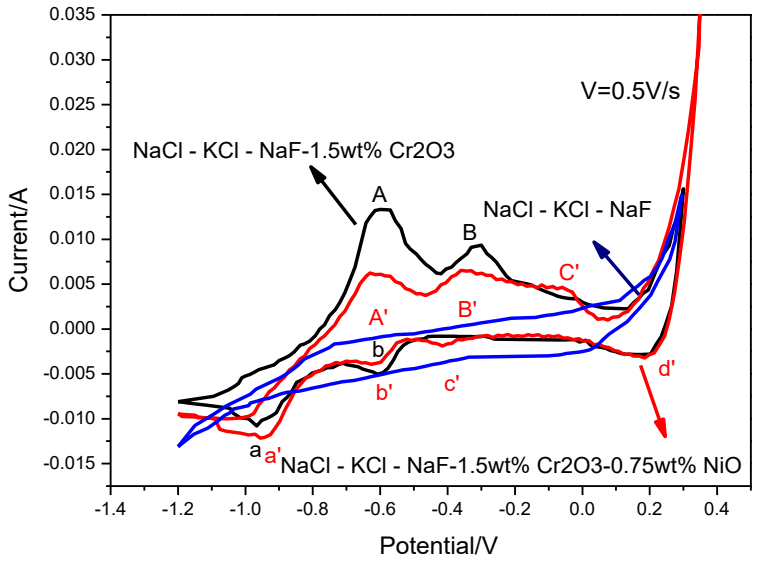

Figure 2. Typical CVs of NaCl-KCl-NaF, NaCl-KCl-NaF-Cr2O3 and NaCl-KCl-NaF-Cr2O3-NiO at 1073 K

Fig. 3 shows the CVs curves for NaCl-KCl-NaF-Cr_2O_3-NiO molten salt at different scan rates between -1.2 V and 0.3 V. The redox peaks a', b', and c' should be attributed to the reductions of Cr(II), Cr(III) and Ni(II), respectively. These peaks appear almost at the same voltage. To verify the reversibility of the cathodic reduction process, the number of discharge steps, and the number of electron transfer, the data of the reduction peaks a', b' and c' were extracted and calculated.

Fig. 4 depicts the relationship between the current density (I_{pc}) and square root of scan rate ($v^{1/2}$) for reduction peaks a', b' and c'. It can be seen that both reduction peaks are almost linear. Therefore, it can be concluded that the reactions of Cr(III), Cr(II) and Ni(II) in NaCl-KCl-NaF-Cr_2O_3-NiO molten salt are reversible reactions[13,14]. The reduction of Cr(III) and Ni(II) is controlled by the rate of electroactive ion diffusion[15]. According to formula $|i_{pa}/i_{pc}| > 1$[16], the cathode product is insoluble**.**

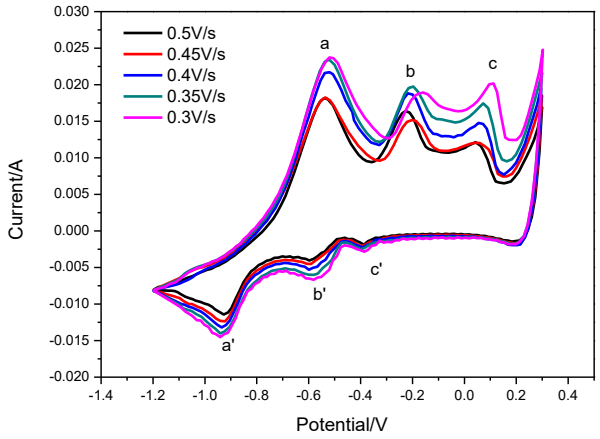

Figure 3. Typical CVs of electrochemical formation in a molten salt at different scanning rates

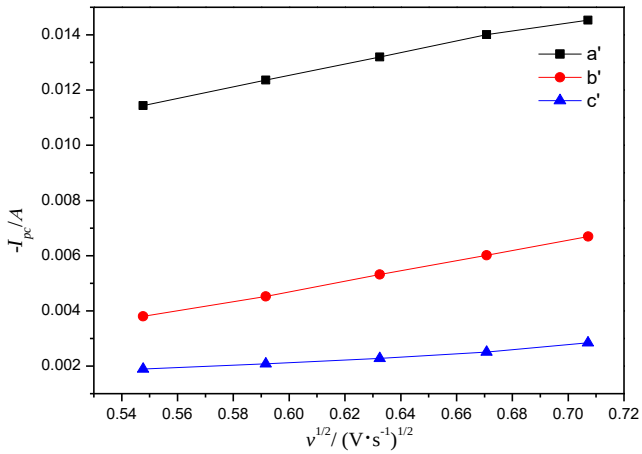

Figure 4. Relationship between I_{pc} and $v^{1/2}$ of peaks a', b' and c'

Assume that the reduction process on the electrode is reversible and the product is insoluble; the experimental data in Fig. 2 are brought into equation (11)[17], which can be used as the basis for judging the reversibility of the corresponding electrochemical reaction[18-20].

$$\varphi_{pc}-\varphi_{pc/2}=-0.77(RT/nF) \qquad (11)$$

The results show that the electron transfer number of the reduction peak b' was 1, and the electron transfer numbers of the reduction peaks a' and peak c' were both 2. Therefore, it can be concluded that the reduction of Cr(III) to Cr during electrochemical reduction takes two steps: $Cr^{3+} + e \rightarrow Cr^{2+}$ and $Cr^{2+} + 2e \rightarrow Cr$, and the reduction of Ni(II) to Ni during electrochemical reduction takes one step: $Ni^{2+} + 2e \rightarrow Ni$.

3.3 Chronopotentiometry

Fig. 5 shows the typical chronopotentiograms of platinum electrodes in the NaCl-KCl-NaF-Cr_2O_3-NiO molten salt at 1073 K. A constant current of 250 mA is applied after 2 s and kept for more than 10 s until the potential becomes 0 V. It shows that there are three jumping platforms in the curve, and their cathode potentials are -0.956 V, -0.607 V, and -0.403 V. This result is the same as the CVs for the cathodic potential reduction process. It can be determined that the b-c platform is the reduction process of Cr(II) to Cr, the d-e platform is the reduction process of Cr(III) to Cr(II), and the f-g platform is the reduction process of Ni(II) to Ni.

When a constant current is applied, the electric double layer of the cathode surface is rapidly charged. Ohmic polarization of the solution on the electrode surface occurs, leading to a sharp potential drop at the instant, as shown in Fig. 5 (a-b). When the voltage increases to -0.956 V, Cr(II) starts to be reduced to Cr. Conforming to the Nernst equation, Fig. 5 (b-c) shows that since the ions of the active particle Cr(II) are reduced to Cr, the concentration of active particles on the surface of the electrode is reduced, and the potential of the electrode is gradually increased. The c-d segment shows that due to the apparent concentration polarization, the electrode potential rises when the concentration of the ion of the active particle Cr(II) cannot maintain the balance between the diffusion rate at the electrode surface and the electrode reaction rate. Then, the new reduction of active particles Cr(III) to Cr(II) starts at -0.607 V, as exhibited in the d-e segment in Fig. 5. When the balance of the diffusion rate and the electrode reaction rate is destroyed, the electrode potential initiates to increase from e to f. The f-g part represents the reduction of active particles Ni(II) to Ni when the concentration of Ni(II) cannot keep the balance of the electrochemical reduction. Finally, the concentration of Ni(II) on the electrode surface decreases to zero, corresponding to location h on the curve.

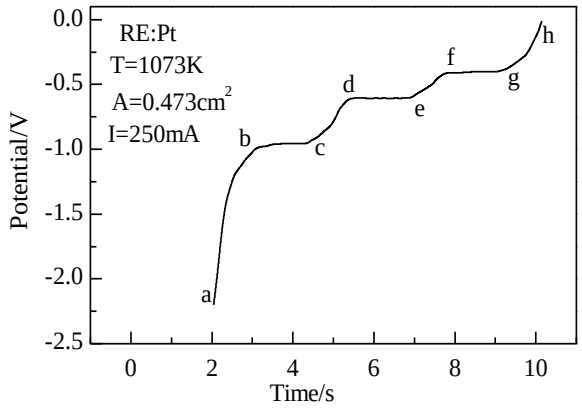

Figure 5. Chronopotentiograms obtained on a platinum electrode in the NaCl-KCl-NaF-Cr_2O_3-NiO molten salt

3.4 Chronoamperometry

Chronoamperometry was used to study the electrochemical nucleation mechanism of nickel-chromium codeposition. The chronoamperometry curve of Fig. 6 is a reduction process controlled by plane diffusion. Three steps occur within the experimental voltage range. According to the result of cyclic voltammetry, the first step in the range of -0.39 V to -0.41 V represents the reduction process of Ni(II) to Ni, the second step in the range of -0.60 V to -0.63 V represents the reduction of Cr(III) to Cr(II), and the third step in the range of -0.95 V to -0.98 V represents the reduction process of Cr(II) to Cr. The potential range of the steps is consistent with the experimental results obtained by cyclic voltammetry. Therefore, when the cathode potential is less than -0.98 V, the codeposition of chromium and nickel can be achieved.

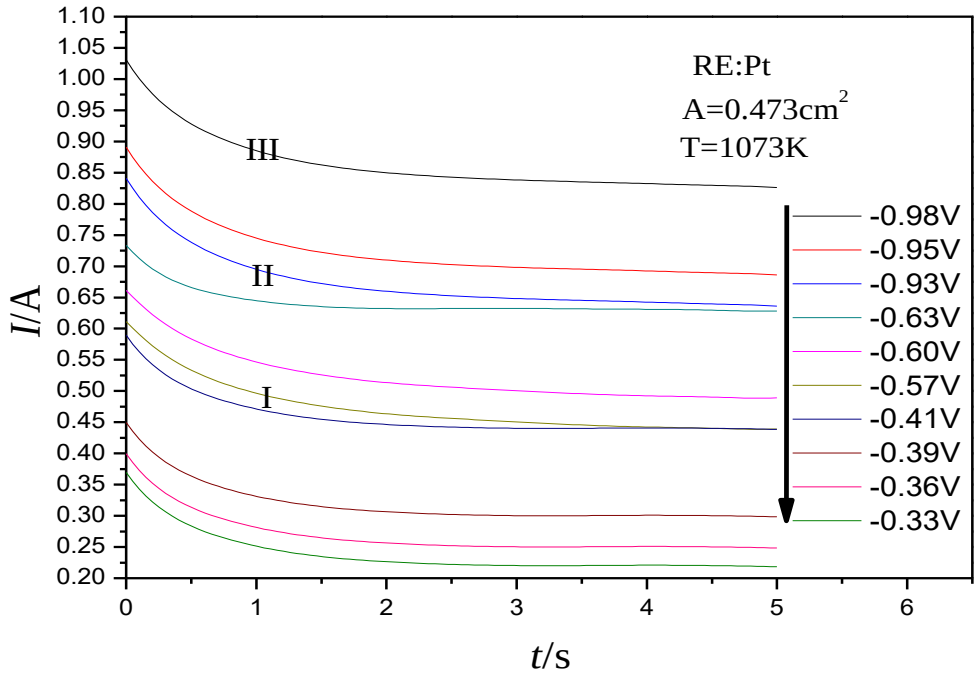

Figure 6. Chronoamperometry curve of Cr-Ni electrochemical reduction

The data obtained by the chronoamperometry method at -0.98 V and -0.41 V in Fig. 6 were respectively calculated[21]. The relationships between I-$t^{1/2}$ and I-$t^{3/2}$ of chronoamperogram at -0.98 V and -0.41 V are shown in Fig. 7, individually.

The relationship between I and t corresponds to equation (12) if the electrocrystallization process is controlled by the diffusion of metal atoms on the surface of the electrode and is a gradual nucleation increase[13].

$$I = \frac{2}{3} nF\pi K_n N_0 (2DC_0)^{3/2} \left(\frac{M}{\rho}\right)^{1/2} t^{3/2} \quad (12)$$

where K_n is nucleation rate constant, N_0 is the maximum possible crystal nucleus density, D is the diffusion coefficient of the electroactive ion, M is the atomic weight of electrodeposit, ρ is the density of electrodeposit, and C_0 is the initial concentration of electroactive ions, respectively.

The relationship between I and t corresponds to equation (13) if the electrocrystallization process is an instantaneous nucleation growth.

$$I = nF\pi N_0(2DC_0)^{3/2}\left(\frac{M}{\rho}\right)^{1/2} t^{1/2} \quad (13)$$

It can be seen that the goodness of fit in Fig. 7(a) and Fig. 7(c) is better. Therefore, the electrocrystallization process of Cr and Ni in NaCl-KCl-NaF-Cr_2O_3-NiO molten salt is an instantaneous hemispheroid three-dimensional nucleation process[22,23].

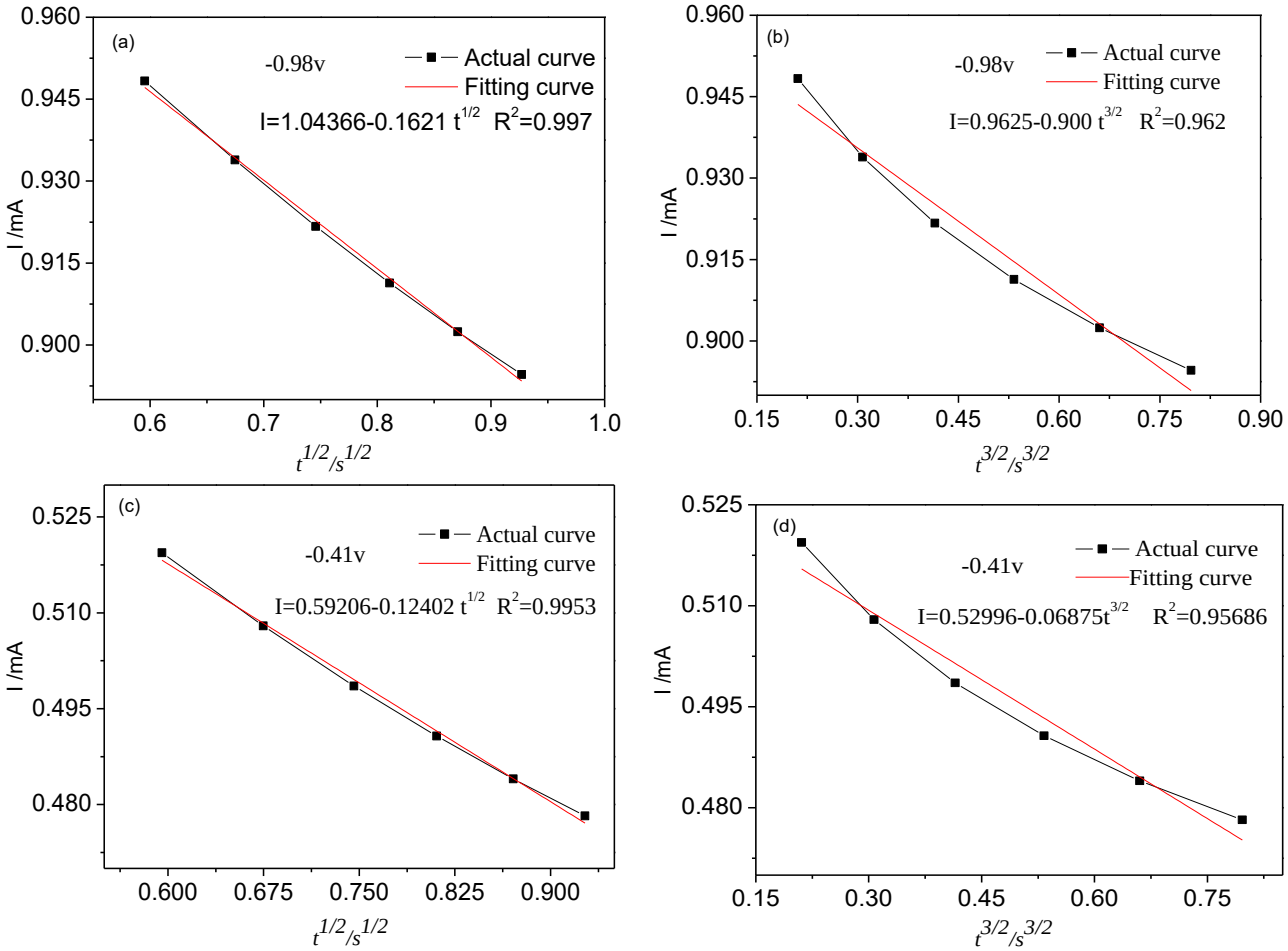

Figure 7. Relationship between I~t1/2(a)(c) and I~t3/2(b)(d) of chronoamperogram at -0.98 V and -0.41 V

3.5 Codeposition and characterization of Cr-Ni alloy coating

The electrodeposition experiments were performed on a platinum substrate in NaCl-KCl-NaF-Cr_2O_3-NiO molten salt at 1073 K with a current density of 300 mA/cm^2 and deposition times of 30 min and 6 h. Fig. 8 shows the surface morphology after deposition. Fig. 8(a) shows that hemispherical three-dimensional nuclear particles of approximately 2-4 μm are attached to the surface of the substrate. The contents of Cr and Ni in the particles were 19.23% and 80.77%, respectively. This confirms that Cr-Ni alloys can be prepared using electrochemical codeposition, and the electrocrystallization process of Cr and Ni is an instantaneous hemispheroid three-dimensional nucleation process.

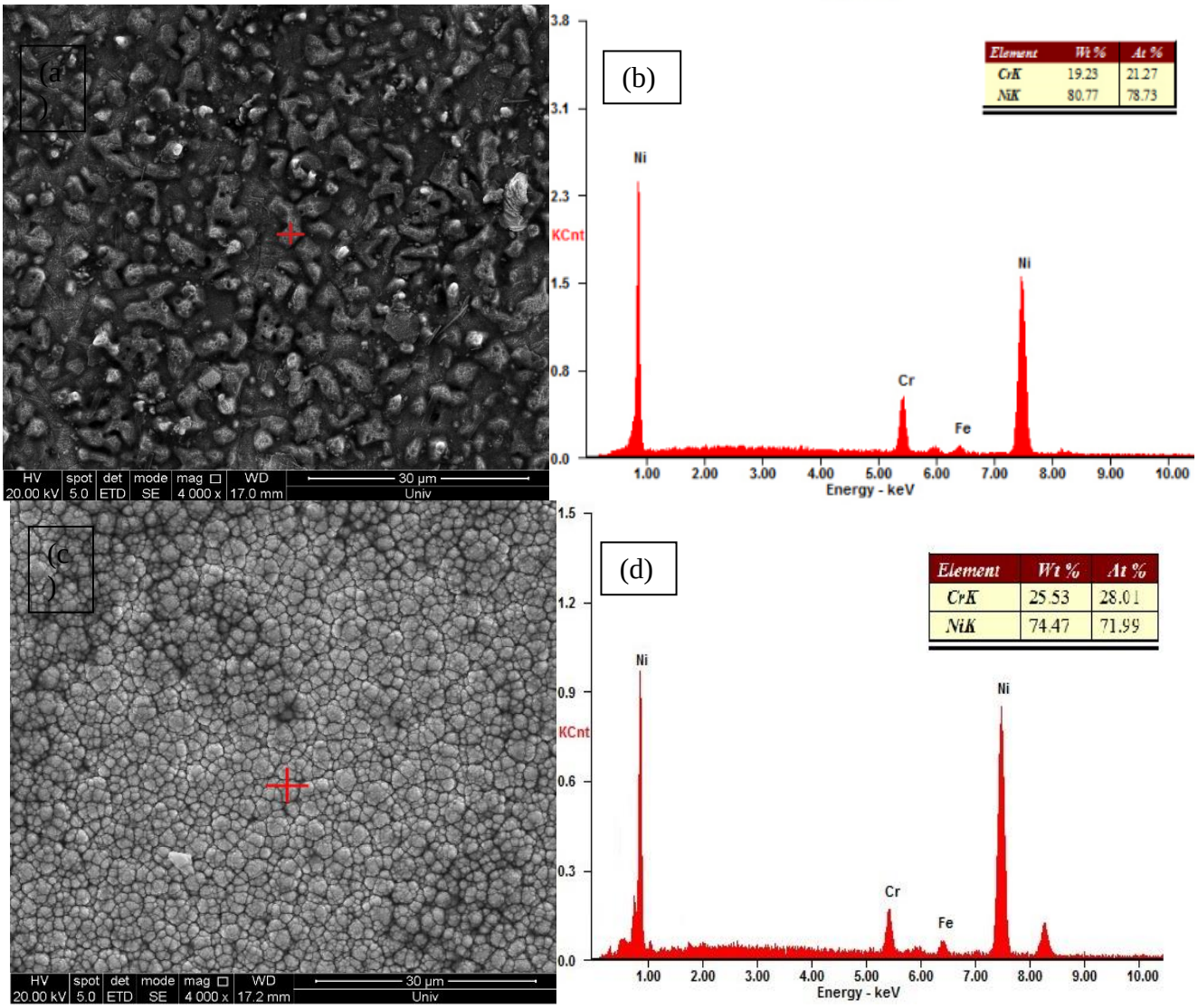

Figure 8. SEM images and EDS tests of the working electrode using constant current electrolysis for 30 min and 6 h

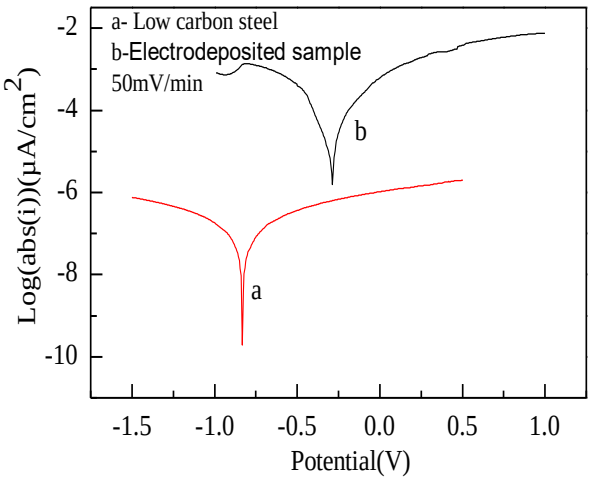

Figure 9. Polarization curves of low carbon steel and electrodeposited alloy coating sample in 3.5% NaCl solution

Fig. 8(c) shows that the deposited layer on the substrate is uniform and smooth, and the grains are fine and regular. The coating has good binding force, and the proportion of Cr and Ni in the particles is 25.53% and 74.47%, respectively.

The corrosion resistance of low carbon steel and chromium nickel alloy containing 25.53% Cr and 74.47% Ni obtained in NaCl-KCl-NaF-Cr_2O_3-NiO molten salt was studied in 3.5% NaCl solution by using the potentiodynamic polarization curve with a scanning speed of 50 $mV \cdot min^{-1}$ at 25°C. The potentiodynamic polarization curves are shown in Fig. 9. The corrosion potential (E_{corr}) and corrosion current density (I_{corr}) of the potentiodynamic polarization curves were extracted out from the original data and listed in Table 1.

Table 1. E_{corr} and i_{corr} of low-carbon steel and alloy coating sample in 3.5%NaCl solution

Sample	E_{corr}/V	$i_{corr\ r}$/A·cm^{-2}
Low-carbon steel	-0.788	-9.722
electrodeposited alloy coating	-0.328	-5.813

The results show that the corrosion potential of the electrodeposited alloy coating sample distinctly moves to the positive direction, and the corrosion current density is much smaller than that of low-carbon steel, which means the corrosion reaction of the alloy coating is much higher, and the corrosion rate is much lower in this medium. This means that the alloy layer is more resistant to corrosion than low-carbon steel.

4. CONCLUSIONS

The electrochemical mechanism and the properties of Cr-Ni alloy coating were studied in NaCl-KCl-NaF-Cr_2O_3-NiO molten salt at 1103 K. According to the studies, the reduction of Cr(III) to Cr during electrochemical reduction takes two steps: $Cr^{3+} + e \rightarrow Cr^{2+}$ and $Cr^{2+} + 2e \rightarrow Cr$, and the reduction of Ni(II) to Ni takes only one step: $Ni^{2+} + 2e \rightarrow Ni$. The electrochemical process of Cr(III), Cr(II) and Ni(II) belongs to reversible reaction controlled by the rate of electro active ion diffusion, and the electrocrystallization processes of Cr and Ni in NaCl-KCl-NaF-Cr_2O_3-NiO molten salt are an instantaneous hemispheroid three-dimensional nucleation process. The compact uniform Cr - Ni alloy coating was successfully prepared via codeposition, and the corrosion resistance of the coating is much higher than that of low-carbon steel obviously.

ACKNOWLEDGEMENTS
The study is financially supported by the National Natural Science Foundation of China (Project No. 51474088), the Hebei Province Natural Science Foundation (Project No. E2016209163, E2017209239), and the Heibei Province High School Science and Technology Research Project (Project No. BJ2017050).

References

1. Manpreet Singh Mrawah, Vajjala Srinivas, Ajoy Kumar Pandey, Shyam Ranjan Kumar, Koushik

Biswas and Joydeep Maity. *J. Iron Steel Res. Int.*, 3 (2011) 72.
2. Zhengwei Liu, Hongling Zhang, Lili Pei, Yilang Shi, Zaihua Cai, Hongbin Xu and Yi Zhang. *J Electrochem. Soc.*, 164 (2017) 237.
3. S. K. Haldar, S. K. Haldar. Platinum-Nicel-Chromium Deposits. *Elsevier Science Publishing Co. Inc.*, (2017) Netherlands.
4. J Park, B Dilasari, Y Kim, K Kim, C Lee and K Kwon. *Mater. Chem. Phys.*, 148 (2014) 444.
5. M Takeuchi, Y Nakajima, K Hoshino and F Kawamura. *J. Alloy. Compd.*, 506 (2010) 194.
6. I Betova, M Bojinov, T Tzvetkoff. *Electrochim. Acta*, 49 (2004) 2295.
7. E L McGinley, D Coleman, G Moran and G Fleming. *Dent. Mater.*, 27 (2011) 637.
8. A. He, J Zeng. *Mater. Design*, 115 (2017) 433.
9. Z. W. Liu, H. L. Zhang, L. L. Pei G. J. Zhu, H. B. Xu and Y. Zhang. *J. Electrochem. Soc.*, 163 (2016) H781.
10. M. Panigrahi, E. Shibata, A. Iizuka and T. Nakamura. *Electrochim. Acta*, 93 (2013) 143.
11. D. Cher, V. Lair, M. Cassir. *Electrochim. Acta*, 160 (2015) 74.
12. R. Giovanardi, G. Orlando. *Surf. Coat. Tech.*, 205 (2011) 3947.
13. A. J. Bard, L.R. Faulkner. Electrochemical Methods - Fundamentals and Applications, Second Edition. *John Wiley Sons, Inc.*, (2001) New York.
14. Donne. S. Supercapacitors: Materials, Systems, and Applications. *Wiley-VCH*, (2013) Germany.
15. M.R. Bermejo, E. Barrado, A.M. Martínez and Y. Castrillejo. *J. Electroanal. Chem.*, 617(2008) 85.
16. Di Li. Electrochemical principles, Third Edition. *Beijing university of aeronautics and astronautics press*, (2011) Beijing (In Chinese).
17. A. M. Abdel-Gaber, B. A. Abd-El-Nabey, I. M. Sidahmed, A. M. El-Zayady and M. Saadawy. *Mater. Chem. Phys.*, 98(2006) 291.
18. Lefrou C, Fabry P, Poignet J. Electrochemistry: The Basics, with Examples. *Wiley-VCH*, (2012) Germany.
19. A. K. Shukla, B. Hariprakash. Encyclopedia of Electrochemical Power Sources. *Elsevier Science Publishing Co. Inc.*, (2009) Netherlands.
20. C Zoski. Handbook of Electrochemistry. *Elsevier Science Publishing Co. Inc.*, (2007) Netherlands.
21. J Wang. Analytical Electrochemistry, Third Edition. *Wiley-VCH*, (2006) Germany.
22. W Schmickler, E Santos. Interfacial Electrochemistry, Second Edition. *Springer*, (2010) Heidelberg.
23. Y Gu, J Liu, S Qu, Y Deng, X Han, W Hu and C Zhong. *J. Alloy. Compd.*, 690 (2017) 228.